J. Mol. Biol. (1979) **130**, 473–492

Three-dimensional Reconstruction of Tubulin in Zinc-induced Sheets

LUKAS K. TAMM, RICHARD H. CREPEAU AND STUART J. EDELSTEIN

Section of Biochemistry, Molecular and Cell Biology
Cornell University, Ithaca, N.Y. 14853, U.S.A.

(Received 14 July 1978, and in revised form 8 January 1979)

The three-dimensional structure of porcine brain tubulin in planar sheets formed in the presence of zinc has been determined to a resolution of approximately 20 Å by electron microscopy and image reconstruction on negatively stained samples. The samples were prepared with a mica floatation technique, which yields tubulin sheets with 36 reciprocal space maxima on lattice lines at 21, 28, 42 and 84 $Å^{-1}$ in Fourier transforms of digitized images. In order to obtain three-dimensional data, sheets were tilted with the goniometer stage of the electron microscope to provide images at various angles between 0° and ±60°. Transforms of 33 tilted images plus the transform of untilted sheets based on an average of nine untilted images were combined to give the third dimension of reciprocal space (z^*). These data were expressed in terms of the phases and amplitudes along the z^* lattice line for each of the 36 maxima observed in untilted samples, as well as five additional lattice lines which have zero-amplitudes in the non-tilted central section of the three-dimensional transform. Some of these zero-amplitudes arise from systematic absences which are due to a 2-fold screw axis relating adjacent protofilaments of tubulin in the zinc-induced sheets. Thus in the three-dimensional reconstructions of the sheets a polarity of the protofilaments is apparent, with adjacent protofilaments aligned in opposite directions to give an antiparallel pattern, in contrast to normal microtubules composed of protofilaments in parallel alignment. Two classes of morphological units, each with a mass corresponding to a molecular weight of about 55,000, are found to alternate along the protofilaments. These distinct morphological units are identified as the α and β subunits of tubulin, confirming the representation of tubulin as an αβ heterodimer. Furthermore, the extensive internal contact between subunits within a dimer can readily be distinguished from the less extensive contact between dimer units. Such differences in contacts were not apparent in the earlier two-dimensional reconstructions. In addition, areas of excluded stain joining one class of subunits to the subunits of the other class in adjacent protofilaments have been resolved for tubulin polymerized in zinc-induced sheets. Of the two classes of subunits one is distinguished by a prominent cleft. Identification of which class of subunits is α and which is β is not yet possible.

1. Introduction

Microtubules play an important role in morphological and dynamic aspects of the life cycle of eukaryotic cells. They are involved in maintenance of cell shape as well as in cellular motility, mitotic division, and transport phenomena. The predominant constituent of microtubules is tubulin, a dimeric protein of 110,000 molecular weight. The two subunits, α and β, appear to be similar in molecular weight (~55,000 each),

0022-2836/79/160473-20 $02.00/0

in amino acid composition and sequence (about 50% homology), in electrophoretic mobility and in their structural features (Grimstone & Klug, 1966; Bryan & Wilson, 1971; Cohen *et al.*, 1971; Chasey, 1972; Luduena & Woodward, 1973). Since the discovery by Weisenberg (1972) of the assembly conditions for microtubules *in vitro*, structural work on microtubules has advanced (Erickson, 1974,1975; Cohen *et al.*, 1975; Mandelkow *et al.*, 1977), with efforts to relate these findings to observations on flagellar microtubule preparations (Amos & Klug, 1974; Amos *et al.*, 1976). Structural investigations by electron microscopy require large, ordered and well-preserved protein assemblies, which microtubules and the microtubule precursor sheets do not usually present. It was therefore a valuable discovery by Larsson *et al.* (1976) that tubulin in the presence of zinc could be polymerized into large sheets. Although the lattice of these sheets is quite different from the normal surface lattice of microtubules (Crepeau *et al.*, 1977), there is the possibility that the subunit arrangement in a single protofilament is similar in the presence or absence of zinc. This view is supported by the observation that the principal effect of zinc is to convert the alignment of protofilaments from a parallel to an antiparallel arrangement (Crepeau *et al.*, 1978; Baker & Amos, 1978).

The studies reported here continue the characterization of tubulin arrays by determining the arrangement of subunits in three dimensions in zinc-induced tubulin sheets. Knowing the relative configuration of tubulin subunits in a zinc sheet will aid in relating this structure to the regular tubular structure. In addition, advantage can be taken of the large ordered array to solve the three-dimensional structure of the two subunits beyond the resolution of about 20 Å reported here by employing the unstained approach of Unwin & Henderson (1975). Furthermore, the properties and behavior of several large microtubule-associated proteins have recently been the subject of intensive examination (e.g. Sloboda *et al.*, 1976; Murphy *et al.*, 1977; Cleveland *et al.*, 1977; Vallee & Borisy, 1978) and structural localization from *in vitro* preparations has been presented (Amos, 1977). Since it is known that microtubule-associated proteins are also involved in zinc sheets (Gaskin & Kress, 1977) progress in the structural analysis of the sheets would also help to clarify the role of associated proteins in the assembly of tubulin arrays.

2. Materials and Methods

(a) *Tubulin preparation*

Microtubules were purified from pig brains by three alternating cycles of depolymerization and polymerization as described by Weingarten *et al.* (1974) and Crepeau *et al.* (1977). The protein was stored at the end of the 2nd purification cycle in liquid nitrogen in small portions for daily use. This material did not lose its activity for at least 6 months. For electron microscopy small samples (0·35 ml) were thawed, diluted 1 : 1 with assembly buffer I (0·1 M-MES†, 1 mM-GTP, 0·5 mM-$MgCl_2$, 1 mM-β-mercaptoethanol, pH 6·4) and subjected to a third purification cycle. After depolymerization of the pellet on ice in the same volume of assembly buffer II (0·1 M-MES, 1 mM-GTP, 1 mM-β-mercaptoethanol, pH 6·4) as the stored sample, the protein was ready for polymerization under various conditions for electron microscopy. The protein concentration at this stage was typically around 4 to 5 mg/ml (Lowry assay, Lowry *et al.*, 1951). Since tubulin is a very unstable protein in its depolymerized state (Weingarten *et al.*, 1974; Crepeau *et al.*, 1977), samples from this solution were prepared within 1·5 h after the last depolymerization step in order to obtain optimal preparations for electron microscopy.

† Abbreviations used: MES, 2(*N*-morpholino)ethane sulfonic acid; EGTA, ethylene glycol bis-(β-aminoethylether)-*N*,*N*′-tetraacetic acid.

(b) *Polymerization conditions*

Tubulin–zinc sheets were usually grown by incubating 60 to 75 μg protein in 100 μl assembly buffer II containing 0·20 mM-$ZnCl_2$ and 0·25 mM-$MgCl_2$ at room temperature for approx. 1 h. Room temperature polymerization proved to yield significantly larger and cleaner sheets than a shorter incubation at 35°C as used previously (Crepeau *et al.*, 1977). Special attention was devoted to the ratio of the concentrations of Zn^{2+} and Mg^{2+} ions. The sheet size was clearly influenced by variation in concentration of either of these divalent cations. Large sheets in both dimensions were only found if [Mg^{2+}] was the same or slightly higher than [Zn^{2+}]. Zn^{2+} concentrations between 0·10 mM and 0·15 mM caused tubulin to polymerize into very long and narrow sheets whereas Zn^{2+} concentrations higher than 0·4 to 0·5 mM led to small sheets. If [Mg^{2+}] was increased without adjusting [Zn^{2+}] sheets were still formed but of smaller size and inferior quality. Although tubulin in polymerized form is considerably more stable than unpolymerized material, sample fixation for electron microscopy by negative stain was completed within 1 h after assembly was completed.

(c) *Preparation of samples for electron microscopy*

Two different techniques were used to prepare negatively stained zinc tubulin sheets. (1) The fast conventional adhesion method on an electron microscope grid coated with a carbon film of medium thickness, and (2) the more complicated mica flotation method described by Horne & Ronchetti (1974) as applied by Crepeau *et al.* (1978). Method (1) was used for fast inspection of polymerization quality, whereas all images used for this analysis were recorded with samples stained by method (2), since sheets prepared in this way exhibited subunit differences and higher resolution.

Since a very thin carbon substrate is used in the mica flotation technique (see below), holey grids were required for support. The holey grids were prepared as described by Pease (1975) and modified by C. Akey in this laboratory. Copper grids (400 mesh) were placed on one end of a microscope slide and dipped at a slight angle into a 4% parlodion solution in *N*-amyl acetate. The slide was pulled out and drained at an angle for several seconds. Shortly before the *N*-amyl acetate was evaporated and the plastic hardened, the slide was held upside down over a steaming water bath which formed small holes in the drying plastic. After examination for quality under a light microscope the coated grids were baked in an oven at 180°C for 30 min and then shadowed with a heavy indirect carbon film, which provides conductivity to the plastic net and prevents it from deteriorating when exposed to the electron beam.

From the best samples of zinc–tubulin sheets, as judged by preliminary examination of normally stained specimens, one drop was placed on a freshly cleaved piece of mica (~2 cm × 2 cm), carefully distributed by tilting, stained with a small drop of 1% uranyl acetate and allowed to dry. Mica sheets prepared in this way were then placed into a vacuum chamber and shadowed indirectly with a thin coating of carbon. Prepared mica sheets could be stored under vacuum for at least one week without loss of quality.

The carbon coated sample was then floated on a solution of 0·5% uranyl acetate. The floating "sandwich" of protein and stain sticking to a thin carbon film was then picked up with a few holey parlodion grids placed on an aluminium screen. The filter paper previously used (Crepeau *et al.*, 1978) often caused shear forces between grid and film by the draining liquid while lifting it up. The grids were carefully dried on filter paper and were then ready for electron microscopy. With this technique a flat protein structure such as tubulin sheet can be stained uniformly on both sides. The continuous support by either mica or carbon provides additional stability to the structure and allows less distortion and disordering of the sample due to drying and handling. The use of this modified Horne and Ronchetti technique provided improved sample preservation in the electron beam enabling the 28 and 84 Å layerlines to be observed at a higher electron dose than reported by Baker & Amos (1978). In addition, 2 to 3 exposures at a magnification of 68,000× could be recorded without significant deterioration in the diffraction pattern corresponding to a cumulative electron dose of about 130 e/Å^2 on the last exposure.

(d) *Electron microscopy*

All micrographs for this work were obtained with a Philips EM301 electron microscope equipped with a eucentric goniometer stage capable of tilts in the range of $-60°$ to $+60°$. The prepared grids were mounted either on a normal specimen holder or, for high tilts and orientation purposes, on a holder with a special device to rotate grids. To avoid unnecessary exposure of the sample to the electron beam, the pictures were taken using a minimal dose technique, as described by Crepeau *et al.* (1977). When a suitable sample was found at low magnification (2600×), its position was recorded on the translation knob that moves the grid nearly parallel to the tilt axis, it was translated, and the objective lens astigmatism adjustments and focusing at operating magnification (65,800×) were done off-sample. After adjustment of the electron beam intensity, the beam was moved out of the viewing area by translating the 2nd condenser lens aperture a calibrated amount. The sample was moved back to its original position, and the electron beam was directed on the sample only after the camera shutter had opened. Thus, it was possible to expose a particular area to the concentrated beam only for the duration of a 2-s period of photographic image recording on a Kodak Electron Image Plate. During a series of pictures of the same sheet, the condenser aperture was immediately closed again and the sample was only viewed at low magnifications between photographs. For maximum speed development in concentrated D-19 an electron dose of approx. 45 e/Å^2 was appropriate. In a preliminary electron dose study it was found that tubulin sheets were largely preserved for about 8 s under these exposure conditions. This meant that only 3 to 4 pictures in a tilt series of the same sheet could be taken without running the risk of obtaining serious radiation damage artifacts. The established procedure was to record at most 3 pictures of the same sheet at different tilt angles followed by one picture at 0° tilt for reference. Usually it was necessary to readjust slightly the position of the sheet between 2 different tilts at low magnification. Whereas the translation along the tilt axis for off-sheet focusing did not affect the underfocus of ~500 to 600 nm (Erickson & Klug, 1971) appreciably, the tilt from one angle to another did, although the tilt axis adjustments on the eucentric stage were made for each grid area again. Therefore it was necessary to refocus for each tilt in a series following the procedure described above. With some practice it was possible to obtain a high percentage of good quality micrographs.

The absolute orientation of the tilt axis on the photographic plate was determined as follows. The height of the specimen holder relative to the tilt axis was misadjusted such that an object moved the distance across the plate when tilted through an angle of approximately $-25°$ to $+25°$. Heavily electron-scattering objects were chosen to tilt through these angles manually while exposing with a very low electron intensity at the same magnification used when images of tubulin were recorded. These plates showed linear streaks perpendicular to the tilting axis due to the movement of the objects during the tilt. With this method the orientation of the tilt axis could be determined to within ±1° accuracy.

(e) *Optical diffraction*

As a simple means for screening large numbers of micrographs, their diffraction patterns were viewed in a vertical optical diffractometer (Crepeau *et al.*, 1977). The best micrographs recorded at tilt angles from 0° to ±60° were selected for computer processing based on their resolution, signal/noise ratio and coherence of the diffraction spots.

(f) *Three-dimensional image reconstructions*

Three-dimensional reconstructions were performed by using the Fourier transforms of tilted sheets to generate phases and amplitudes along the z^* axis for each Fourier space maximum, as proposed by DeRosier & Klug (1968) and carried out by using different projections from tilted micrographs by Crowther *et al.* (1970). These techniques were first used for 2-dimensional protein arrays (unstained purple membrane) by Henderson & Unwin (1975). The computations were performed by our laboratory computer system, which consists of 2 minicomputers, a Data General Nova 1200 with 32K words of memory and a Data General Eclipse S/130 run as a mapped system using 64K 16-bit words of semiconductor memory. Each unit operates in conjunction with 2 disk drives (5 megabytes storage capacity for the Nova and 10 megabytes for the Eclipse). Disks are used for

storage of programs and temporary storage of data. Linkage between the 2 systems is accomplished by a magnetic tape drive, which is also used for permanent data storage. Each computer is operated through a Tektronix graphics terminal, which allows use of the computer system in a fast interactive mode. Electron micrographs are digitized with a Syntex AD-1 autodensitometer. Programs for 2-dimensional image reconstruction are based on the methods of DeRosier & Klug (1968) as modified by Gene Dykes for our laboratory computer system. A phase search program taking rotational and screw symmetry elements into account allowed us to average several sheets (Crepeau *et al.*, 1978) and provided information about the orientation of a sheet on the electron microscope grid and the presence of symmetry relations in 2 and 3 dimensions.

(g) *Initial characterization of the sheets*

The basic method for generating a 3-dimensional Fourier transform of the 2-dimensional protein array is to combine sections through the transform at various tilt angles after a common phase origin for each section has been found. The individual sections are obtained from 2-dimensional transforms of projections of the tilted object. This method is justified, since the depth of focus in an electron microscope is much larger than the sample thickness and one therefore is always dealing with transforms of true projections. Using this approach, it is possible to partially fill the 3-dimensional Fourier space by beginning with the maxima of the transform of the non-tilted projection, then adding data from lower tilt angles for the various z^* lines and finally completing the process with data from the highest tilts.

In order not to propagate errors we wanted to be certain that the transform maxima of our planar data set ($z^* = 0$) was well defined, since it is these data upon which all the later phase searches depend. It was especially important to be careful at this stage, since some maxima included in this analysis have amplitudes only slightly above noise level. We therefore averaged the transforms of 9 different micrographs, taken at 0° tilt, for our 3-dimensional transform section. The results of that work have been published in an earlier paper (Crepeau *et al.*, 1978). From that study it also emerged that there is a 2-fold screw axis present in a zinc-induced tubulin sheet projected into 2 dimensions. Implications of this screw axis will be carried along and elucidated in more detail in this work.

Before further work could be planned 2 important points needed to be clarified. (1) The minimal number of views required for a 3-dimensional reconstruction to 20 Å resolution; and (2) whether the screw axis is also present in 3 dimensions. In regard to the first point, it is known from Fourier theory, that the convolution of the transform of the 2-dimensional periodic structure with the thickness of the sheet restricts the maximal possible phase change across z^*, particularly for high amplitudes. The thickness of a zinc-tubulin sheet was initially estimated to be 70 to 80 Å according to measurements on microtubules by electron microscopy (Amos & Klug, 1974) and X-ray diffraction (Mandelkow *et al.*, 1977). Calculation with these numbers predicts a smooth phase variation over about 1/50 Å, or $\pm$ 1/100 Å in either direction from an established data point. Therefore, in the worst case, each succeeding section should intersect a high resolution (1/18 Å) lattice line within a distance of 1/100 Å. This condition is satisfied when successive tilt angles are within 10° ($\tan 10^\circ \approx \frac{1}{100}/\frac{1}{18}$). Images were usually recorded at random orientations of the sheet with respect to the tilt axis. On average, 2 sheets roughly perpendicular to each other at each tilt angle were considered as sufficient. The tilt stage allows tilts from $-60°$ to $+60°$, and one therefore calculates 24 independent views are needed for a reconstruction of 20 Å resolution, several more than indicated by the considerations of De Rosier & Klug (1968). However, we were aware that frequently a reflection may be swamped by noise and some redundancy is in order. In fact, we used 33 tilted micrographs and 9 at zero degree of tilt. Further confidence that sufficient data were collected is gained because the presence of the screw symmetry has not been introduced in the calculation of the required number of views and hence we have another safety factor of 2. Because of the limited tilting capacity, one loses all the information contained in a cone from 60° to 90° in the 3-dimensional transform. This is negligible for most lattice lines, since the data cut-off is beyond the resolution limit. By restricting the few reflections closest to the origin towards high z^* values one might lose some resolution in the z dimension.

In regard to the issue of the screw axis, analysis for its presence in 3 dimensions was

performed on a sheet tilted 20° with the tilt axis almost perpendicular (8° off) to its protofilaments or parallel to the presumed screw axis (Fig. 1). In order to describe the restrictions imposed on the Fourier transform by a symmetry operation one can perform the operation on the object in real space (in our case a rotation of 180° followed by a translation of half a unit cell) and if the symmetry is present the object will be unchanged. In Fourier space one may also perform the symmetry operation and by requiring the Fourier transform to remain unchanged as the real space object was unchanged we arrive at the restrictions on

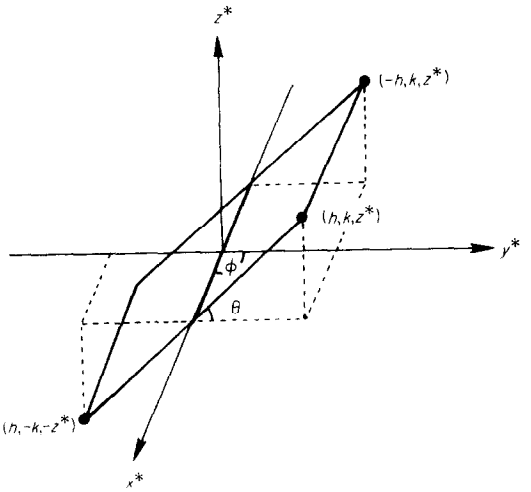

FIG. 1. Tilted plane which represents a section through Fourier space. In this particular case, where the tilt axis lies along the x^* axis of the transform (h,k,z^*) and $(-h,k,z^*)$ can be compared on the same 2-dimensional transform section and tested for a possible 3-dimensional 2-fold screw axis (see text). h,k and z^* are co-ordinates in Fourier space, θ is the tilt angle and ϕ designates the orientation of the tilt axis relative to the protofilament axis (y-co-ordinate in real-space).

the transform required by the symmetry. The operation of a screw axis in Fourier space is a 180° rotation about the axis (h) followed by a phase shift of $h\pi$ for a reflection (h,k,z^*) corresponding to the translation of one half a unit cell in the h direction. In other words reflection (h,k,z^*) must equal reflection $(h, -k, -z^*)$ with a phase shift of $h\pi$. Since $(h, -k, -z^*)$ is related to $(-h, k, z^*)$ by Friedel's law and if we represent amplitude and phase A and ϕ, respectively, we may write

$$A(h, k, z^*) = A(-h, k, z^*)$$

and

$$\phi(h, k, z^*) = -\phi(-h, k, z^*) + h\pi. \tag{1}$$

Here we have used Friedel's law which relates 2 centrosymmetric maxima S and S' in a Fourier transform of a real object as follows: $A(S) = A(S')$ and $\phi(S) = -\phi(S')$. In the case of the zinc-induced tubulin sheet tilted 20°, a given point (h, k, z^*) is first rotated into $(h, -k, -z^*)$ by the 180° rotation about the axis parallel to h in Fourier space. Point $(h, -k, -z^*)$ is centrosymmetric to $(-h, k, z^*)$ and therefore these 2 points are related by Friedel's law. For maxima on the meridian this relationship reduces to $\phi(0, k, z^*) = -\phi(0, k, z^*)$ with the two unique solutions $\phi = 0°$ or $\phi = 180°$ for any k and z^*. Maxima on the equator with odd index h have to satisfy the equation $\phi(h, 0, z^*) = -\phi(-h, 0, z^*) \times \pi$. If $z^* = 0$, the 2 phases become Friedel-related, which is incompatible with the requirements of the screw axis, and as a consequence there is a zero amplitude or systematic absence at $(h, 0, 0)$ when h is odd. Choosing a sheet tilted about the screw axis (h) ensures screw-related reflections at $(\pm h, k, z^*)$ will be present. By running a phase search program, which compared the screw axis-related maxima on this particular sheet tilted nearly on its screw axis, we found a phase origin that gave an average deviation of 19° from the phases expected

with the screw axis for 8 pairs of maxima and 3 single meridional maxima. Since this average deviation is of the same order as obtained for fitting non-tilted sheets to each other, we concluded that the screw symmetry is present in 3 dimensions, as well as previously found for the 2-dimensional projection.

(h) *Construction of the three-dimensional transform*

For the final analysis micrographs recorded at tilt angles from 10° to 60° and at many different orientations with respect to the tilt axis were processed along with the data at zero degrees of tilt. Selected examples of images and their optical transforms are shown for an untilted sheet, a sheet at moderate tilt and a sheet at high tilt in Figs 2 to 4, respectively. Fig. 2(a), taken at zero tilt, shows the standard appearance of a zinc-tubulin sheet and the optical diffraction pattern. Fig. 2(b) illustrates the systematic absences along the $k = 0$ line. In the average of 9 sheets at zero degrees it was established that the (0, 1) spot is absent (though not due to a symmetry) and the (0, 2) reflection is weak (present in 4 out of 9 sheets). (Additional comments on the (0, 2) z^* lattice line are made in regard to Fig. 5.) A study of the phases established the existence of $p1g1$ symmetry of the untilted sample. The micrograph in Fig. 3(a) taken at a moderate tilt angle of 30° appears similar to that in Fig. 2(a) with the exception that the protofilament pairing is faintly visible. The diffraction pattern (Fig. 3(b)) shows the deviation from the orthogonal relation between the lattice lines apparent in Fig.2(b) due to the tilt and the appearance of the (1, 0) and (3, 0) reflections that were systematic absences in Fig. 2(b). Also the (0, 2) reflection is evident. Fig. 4(a) at a large tilt angle of 55° shows the problems of microscope focus present in tilted specimens. The sequence proceeds from overfocus to underfocus from bottom to top of Fig. 4(a). The area used for the optical and more importantly the computed transform was selected in a region where the focus is such that the transfer function is flat to beyond the cut-off in the crystal reflections. Corrections as employed by Henderson & Unwin (1975) were found to be unnecessary due to the strength of the diffraction pattern from limited areas and the relatively poor resolution with negative stain. The diffraction pattern of Fig. 4(b) again shows the features of a tilted specimen with the spreading in the k direction limiting the pattern to 2 lattice lines or about 31 Å resolution. In examining the optical diffraction patterns it should be noted that we found in general the resolution is better in a computed transform and thus for the example in Fig.2(b) all 36 reflections found at zero tilt in the average of 9 transforms are not present in this Figure. The reflections used in the final reconstruction consist of 6 independent reflections on $k = 0$; 9 on $k = 1$ from $h = -4$ to $h = 4$; 13 on $k = 2$ from $h = -6$ to $h = 6$; 5 on $k = 3$ from $h = -2$ to $h = 2$; and 8 on $k = 4$ from $h = -4$ to $h = 4$ excluding $h = 0$. The $z^* = 0$ section has the above excluding 3 odd reflections on $k = 0$ and the reflections (0, 1) (not observed) and (0, 2) judged to have zero amplitude due to the rapid phase shift (see Fig. 5(c)). For all of the images the computed 2-dimensional Fourier transforms were reduced to peak amplitudes and phases at exact lattice points where the amplitudes were significantly above the noise level. In order to determine the correct 3-dimensional position of each view, a reference plate for the same sheet at 0° tilt was analysed. Its transform was checked in a phase search program for the 2 possible orientations of the projection of a sheet with 2-fold screw ($p1g1$) symmetry.

These 2 orientations are related by a 2-fold rotation to each other. Thus, either case 1 or 2 could be assigned to each tilt, determining its exact position in 3 dimensions, because the 2 angles of tilt and orientation were known. An exact z^* value for each maximum on the transform of each sheet could be computed from:

$$z^* = \left(\frac{k}{84}\sin\phi - \frac{h}{96}\cos\phi\right)\tan\theta, \tag{2}$$

where 96 and 84 are the unit cell dimensions (in Å) for h and k in the untilted projection, θ designates the tilt angle of the goniometer stage and ϕ corresponds to the orientation (rotation) angle of the protofilament axis of the sheet with respect to the tilt axis. For case 2 the value of z^* must be multiplied by -1.

The next step in the reconstruction process was to find a common phase origin for every section and then to combine them in 3-dimensional Fourier space. These 2 operations were

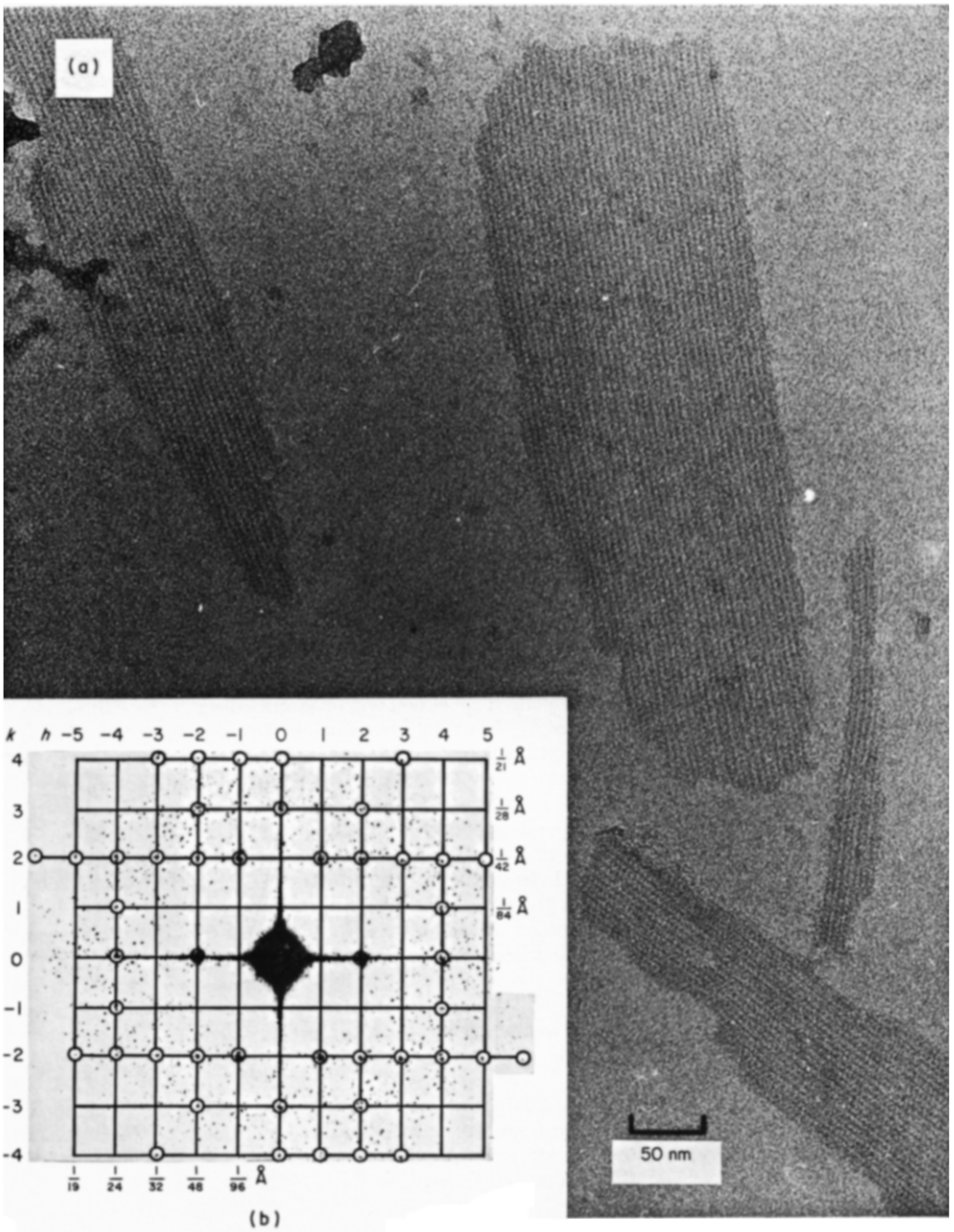

FIG. 2. Untilted zinc–tubulin sheet. (a) Electron micrograph of a sheet with longitudinal striations representing individual protofilaments (40 or more in larger sheets). The protein was negatively stained with uranyl acetate using the mica flotation technique described in Materials and Methods. (b) Optical transform of the large sheet in (a). The reciprocal lattice lines indicate reflections arising from the regular sheet structure. The transform was recorded with the equator ($k = 0$) oriented perpendicular to the sheet shown in (a) and the brightest spot (2,0) corresponds to the protofilament spacing of 48 Å. Note the systematic absences of (1,0) and (3,0).

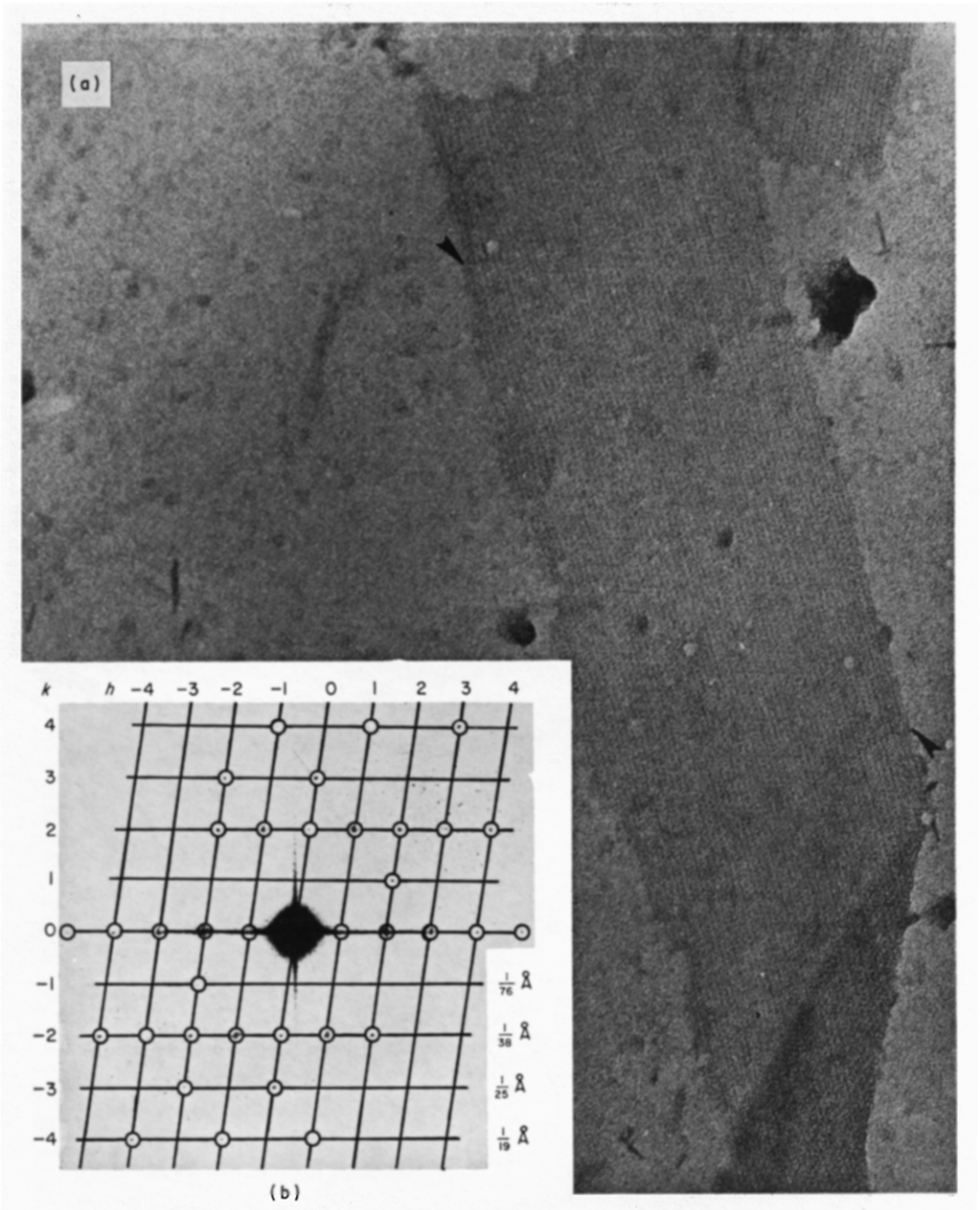

FIG. 3. Zinc-tubulin sheet tilted 30°. (a) Electron micrograph of a zinc-induced tubulin sheet tilted 30° using the goniometer stage of the electron microscope. The tilt axis (arrows) lies at an angle of 30° to the protofilaments of the sheet. (b) Optical transform of the sheet in (a). The lattice lines are no longer rectangular due to a tilt on an axis neither parallel nor perpendicular to the sheet. Because of the smaller spacings of the projection of the tilted sheet, the reciprocal lattice lines increase to multiples of 1/76 $Å^{-1}$ instead of 1/84 $Å^{-1}$ in the normal view (Fig. 2).

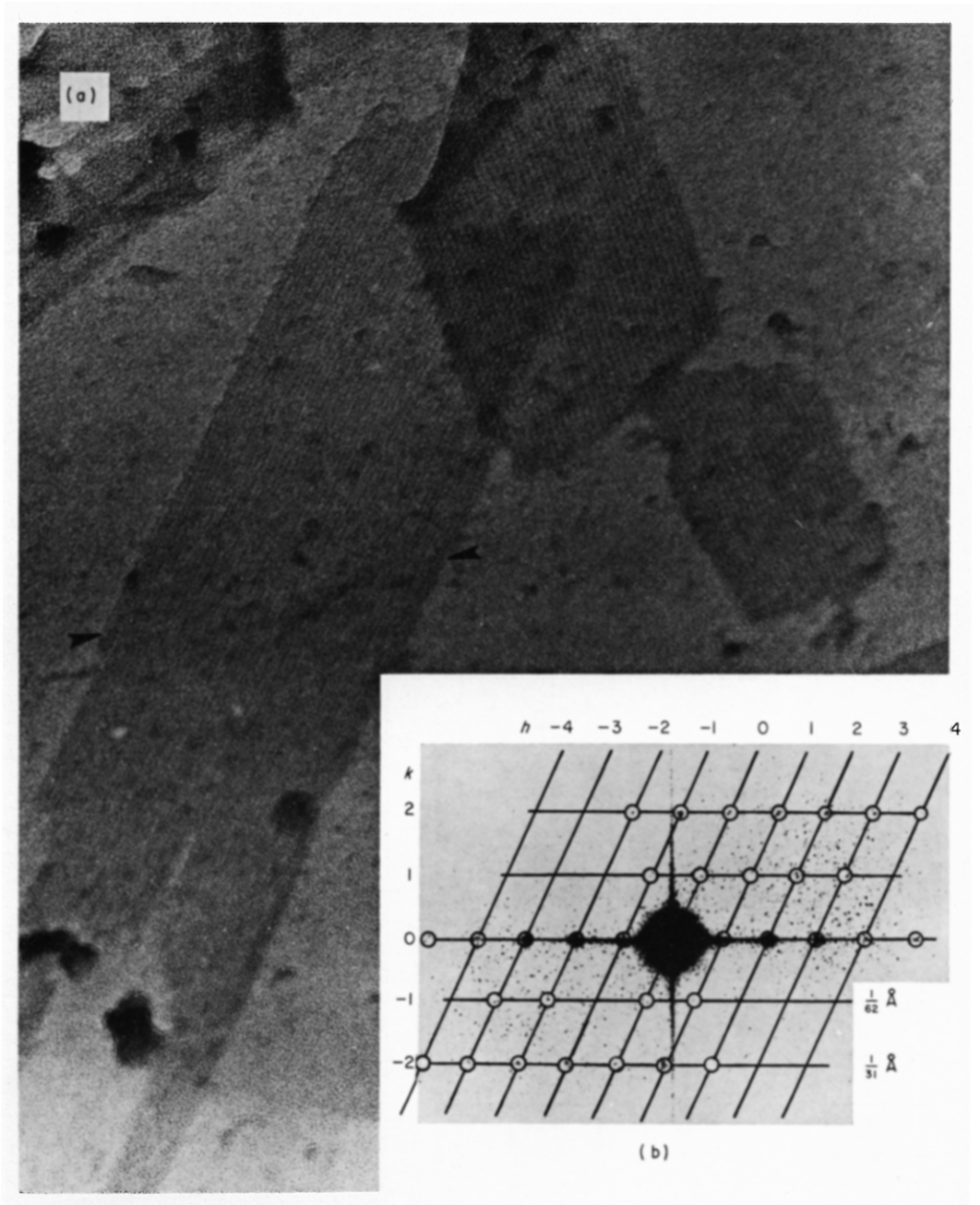

FIG. 4. Zinc-tubulin sheet tilted 55°. (a) Electron micrograph of a zinc-induced tubulin sheet tilted 55° with the goniometer stage of the electron microscope. The tilt axis (arrows) lies at an angle of 51° to the protofilaments of the sheet. A strong pairing of protofilaments is apparent due to a staggering of alternating protofilaments. A change of focus because of the high tilt angle is visible, progressing from overfocus (lower corner on the left) through focus to underfocus (top of the micrograph). (b) Optical transform of the sheet in (a). In this case the reciprocal lattice lines increase due to the tilt to multiples of 1/62 $Å^{-1}$. The higher-order k lattice lines are beyond resolution. The strong reflections appearing on (1,0) and (3,0) originate from the pairing of protofilaments in (a).

done simultaneously in an iterative manner, building up the 3-dimensional transform sequentially by sections from the 2-dimensional transforms of images recorded at increasing tilt angles. Therefore, whenever a section was found to fit, it was added to the existing 3-dimensional transform, contributing to the "template" to which the next section at a higher tilt could be fitted. The initial section was the average of 9 zinc sheets in the $z^* = 0$ projection (see above). The program to generate the 3-dimensional transform works in 3 steps. (1) Selection of the unused section closest to the existing 3-dimensional transform; (2) searching for the phase origin of the section with the smallest residual phase differences with reference to the 3-dimensional transform and scaling of the amplitudes; and (3) adding the new section to the 3-dimensional transform data set. Phase fitting was done including a weighting factor for strong amplitudes in consideration of the susceptibility of weak maxima to random noise and the distance on the z^* line to the next available data point in the 3-dimensional transform. Since phase changes along z^* must be allowed, a particular maximum was neglected in the fitting process if it was not within $3/256$ Å^{-1} of the closest data point but, once the proper phase origin was found, this point could be included into the 3-dimensional transform without any restriction.

The program for establishing the complete 3-dimensional transform was run interactively allowing reflections to be omitted for either phase search or addition to the transform or both. The same program served for refinement of the phases in a 2nd cycle, with the whole 3-dimensional transform data block obtained in the 1st cycle minus the tilt under consideration serving as a template. This refinement was especially helpful, since our basic strategy was to include as many maxima as possible in the 2-dimensional transforms of the individual sections and to eliminate noise in the process of constructing the 3-dimensional transform. Therefore about 20 to 30% of the weaker maxima, especially on the 1st and 3rd lattice lines ($k = 1, 3$), were discarded at this stage, whereas the stronger reflections in general showed very good consistency. By running through more than one cycle, by smoothing amplitudes and phases along the z^* axis and finally by introducing the 2-fold screw axis (see below), a set of amplitudes and phases was determined even for spots of relatively low intensities.

Since smooth and continuous amplitudes and phases sampled at 32 discrete points along a z^* line are required for the inverse Fourier transform, a program was designed to approximate the data obtained in the previous program with a smooth curve. This was done for amplitudes and phases, with real and imaginary parts in the case of phases smoothed separately (to avoid the discontinuity from 360° to 0°). Some examples of interest are shown in Fig. 5. These include the (2, 0) lattice line with a strong maximum at $z^* = 0$ corresponding to the spacing of protofilaments (Fig. 5(a)), the (3, 0) lattice line with the systematic absence at $z^* = 0$ (Fig. 5(b)), the (0, 2) and (0, 3) lattice lines (Fig. 5(c) and (d)), the strong (1,2) lattice line (Fig. 5(e)) and the weak (1,4) lattice line (Fig. 5(f)). The curves of Fig. 5 were computer drawn with circles in the amplitude and phase curves representing actual data points obtained by averaging all the sheets contributing to that specific z^* value. The dots represent interpolated values required by the curve smoothing program.

(i) *Application of the 2-fold screw axis*

Since the initial characterization of the zinc-induced tubulin sheets indicated a 2-fold screw axis perpendicular to the protofilaments, the screw axis was reconfirmed for the completed 3-dimensional transform. In the amplitude/phase *versus* z^* plots of Fig. 5 the presence of such a screw axis is evident. For example maxima (1, 0) and (3, 0) show amplitudes dropping to zero when $z^* = 0$ (the latter is shown in Fig. 5(b)), as required because of the systematic absences. The $k = 0$ maxima (0, 1), (0, 2), (0, 3) could be fitted to either 0° or 180° (the latter 2 are shown in Fig. 5(c) and (d), respectively), the errors being within experimental accuracy. An interesting feature is that 2 of these maxima ((0, 2), Fig. 5(c) and (0, 1), not shown) change their phase at $z^* = 0$ from 0° to 180° and have therefore very low amplitudes in this region of transition. They were not observed consistently in untilted 2-dimensional projections, whereas the 3rd one (0, 3) was always present in non-tilted transforms with a strong amplitude and a phase close to 180° (Crepeau *et al.*, 1978). In the untilted sheets the (0, 2) reflection was previously judged to be weakly present on the basis of 4 out of 9 sheets (Crepeau *et al.*, 1978). However, when the phase behavior of

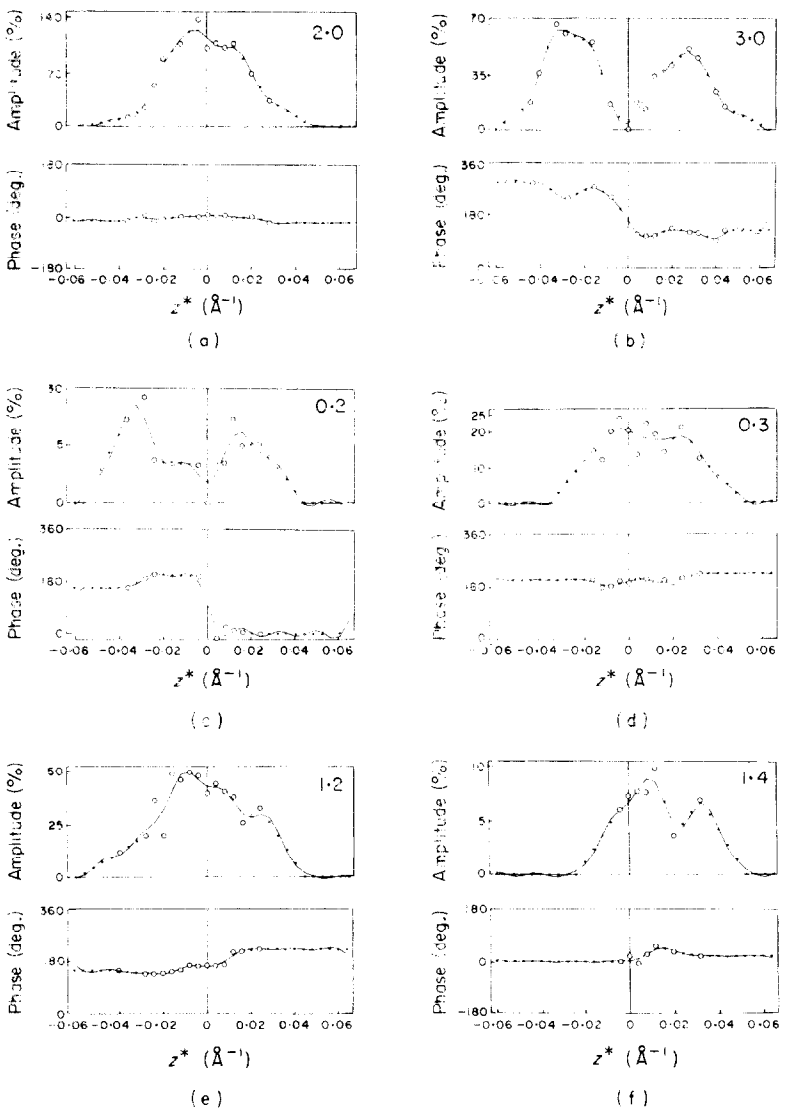

FIG. 5. Amplitudes and phases along z^* lattice lines of the 3-dimensional transform, for 6 positions of the transform of untilted sheets. All amplitudes are scaled to the $z^* = 0$ value of (2,0), which is 100%. Indexing is as in Fig. 2(b). The data presented here are the raw data before the symmetry constraints are applied. Circles represent the actual data in the amplitude curves and may be an average from more than one sheet, while dots represent interpolated points where no data were available. The smooth curves are computer generated and, with the exception of the $z^* = 0$ point which was not allowed to change, were used in subsequent processing.

(a) 2nd equatorial maximum (2,0) at 1/48 Å^{-1}, the spacing of protofilaments. Phases and amplitudes are symmetric for positive and negative z^* values.

(b) Maximum (3,0) which has low amplitudes near $z^* = 0$, indicating the systematic absence for that spot in transforms of normal projections as required by the screw axis. The amplitudes and phases obey the screw relationship $\phi\,(h,0,z^*) = \phi\,(h,0,-z^*) + \pi$, within experimental error.

(c) Maximum (0,2) on the meridian. The phases are either 0° or 180° (screw requirement) and have a rapid transition at about $z^* = 0$. Such a change in phase can only occur if the amplitude is very low (see text).

(d) The 3rd meridional maximum (0,3), which was always observed to be relatively intense at low tilt angles. The phases are near 180° and fulfil the requirements for the screw axis.

(e) Maximum (1,2) which is one of the most intense maxima of transforms at all tilt angles.

(f) Maximum (1,4). Such high resolution maxima are only measured at relatively low z^* values, since their values on high tilts are outside the resolution limit of 1/18 Å.

Fig. 5(c) for this reflection is examined it is evident that the amplitude must be small around $z^* = 0$ and for the 3-dimensional reconstructions an amplitude of zero was assigned to the point $z^* = 0$. Throughout the whole tilt range, a phase of 180° can be assigned to the (0, 3) lattice line (Fig. 5(c)). Further indications of the screw axis are the symmetric phases of even-numbered $h = 0$ maxima, such as the strong (2, 0) maximum (Fig. 5(a)) and the (4, 0) maximum (Figure not shown).

Since the presence of a 2-fold screw axis was indicated, a 3-dimensional transform data set with an enforced screw axis was generated by averaging screw-related data points and compared with the directly obtained data. In general quite good agreement was obtained between the raw data and the smoother symmetry enforced data set. The root-mean-square phase error, defined as

$$\epsilon_a = \left[\frac{1}{N}\sum_{i=1}^{N} (\text{observed phase} - \text{calculated phase})^2\right]^{1/2}$$

was 20° and the R factor, defined as

$$R = \frac{\sum_{\text{all spots}} |\text{amplitude observed} - \text{amplitude calculated}|}{\sum_{\text{all spots}} |\text{amplitude observed}|},$$

was 0·16. The average phase error was 14°. High phase discrepancies in a few cases could be eliminated by discarding one possibly erroneous point. The screw averaging was also very helpful in providing data for areas of the 3-dimensional transform that had been rather poorly documented. The screw relation could be introduced either before or after smoothing the data with essentially the same effect. However, application of the screw axis after smoothing allowed us to use the given data much more efficiently, since it could also be compared in interpolated regions. Subsequently, the 3-dimensional Fourier transform, consisting of 41† continuous lattice lines along z^* which are distributed at discrete points on the 4 reciprocal lines corresponding to spacings of 84 Å^{-1}, 42 Å^{-1}, 28 Å^{-1} and 21 Å^{-1} (see also Fig. 2(b), was subjected to an inverse Fourier transformation using a $32 \times 32 \times 32$ matrix to obtain a 3-dimensional reconstruction for one unit cell.

3. Results

The three-dimensional reconstruction may be viewed at any angle as a series of sections perpendicular to the protofilaments outlined at a constant contour level and stacked with hidden contour lines removed by the computer. Figure 6(a) and (b) presents two representative views of a three-dimensional reconstructed image made up of four unit cells. The outlines for the two types of morphological units are clearly seen alternating along each protofilament as distinct and slightly elongated globular structures. Presumably these morphological units correspond to the α and β subunits of tubulin, although specific identification is not possible. Figure 7 shows a projection of the three-dimensional structure perpendicular to the plane of the sheet. This may be calculated from either the zero degree data or from the projection of the full three-dimensional structure. This Figure is very similar to that of Crepeau *et al.* (1978) and is in agreement with that of Baker & Amos (1978). If the contour lines are extended into the region between the protofilaments, the connections noted by Baker & Amos (1978) are seen in the same places (A, B and C of Fig. 7). Sections through the sheets at positions indicated in Figure 7 are given in Figure 8(b) to (d). The contour levels in these Figures are chosen to emphasize points of interest and are not equal in different Figures. The adjacent protofilaments are well separated and are staggered relative to each other across the zinc-sheet. One is centered above the central plane of the sheet,

† Four high resolution spots were only observed in the central section.

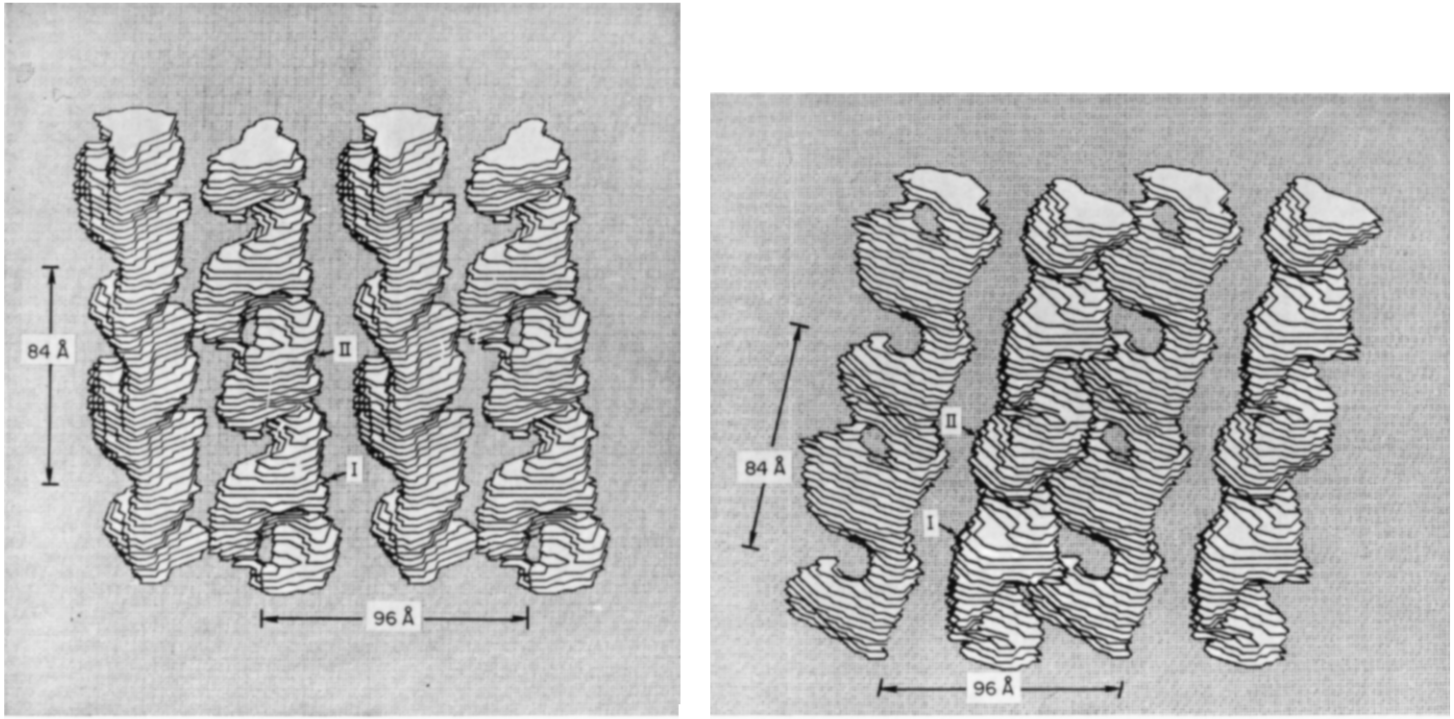

FIG. 6. Three-dimensional reconstructions of the zinc-induced tubulin sheets. Four protofilaments are shown, each for a length of 2 unit cells terminating at top and bottom at the screw axis. The reconstructions are viewed looking approximately toward the positive z axis with the x axis to the right and the y axis downward. The contour level has been chosen to emphasize the shape of the protofilaments. Screw axes are present at the top and bottom of the Figure and every 42 Å along the protofilaments.

(a) Three-dimensional reconstruction viewed almost face-on, tilted 25° and rotated 10° to bring the rightmost protofilament above the plane of the picture. The triangular shape of the protofilaments suggests a packing arrangement in a microtubule in which the vertex of the triangle is pointing inward giving rise to the curvature of the microtubule wall. Subunits are labeled I and II to facilitate comparison with subsequent Figures. The long axis of subunit I lies at an angle of about 30° from the protofilament axis and about 30° out of the plane of the sheets.

(b) Three-dimensional reconstruction viewed from an angle about 30° to the side and 30° out of the plane. The left-hand protofilament is above the plane of the Figure. The staggering of 2 adjacent protofilaments is evident in this view. This same effect causes the pairing of the protofilaments in Fig. 4(a).

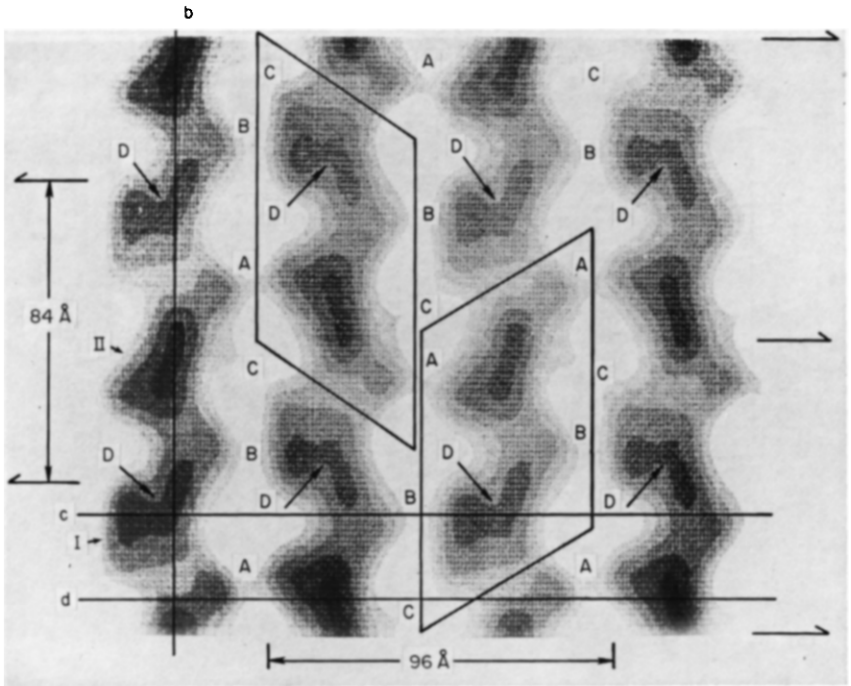

FIG. 7. Projection of 2×2 unit cells of a zinc-tubulin sheet on to a plane. This 2-dimensional projection is generated either by an inverse Fourier transform of the central section of Fourier space or by projecting the whole 3-dimensional reconstruction on to a plane. The different shapes of the 2 classes of subunits are due to α–β differences which include inequivalent 3-dimensional arrangements. The probable $\alpha\beta$ dimer units based on stain penetration are enclosed in boxes. The 2 screw axes of each unit cell are marked by arrows on either side of the projected reconstruction. Regions of interest are labeled A through D and include regions of contact between protofilaments, A and B being stronger contact regions and C being a weak region not clearly evident at this contour level (see Baker & Amos, 1978). D indicates a cleft in the I subunit. Small letters b, c and d refer to the location of sections of the reconstruction perpendicular to the plane of the sheets shown in Fig. 8(b), chosen to show features A through D.

the next below and so forth, giving the impression of a pleated structure with a folding angle close to 150° and a staggering of about 15 Å. This staggering is evident in Figure 6(b). The whole sheet is approximately 80 Å thick, and the individual subunits span a distance of about 60 Å across the sheet (see Fig. 8(b) to (d)).

Since stain cannot penetrate easily into very close intermolecular contacts, the single protofilaments appear as solid tubes. Nevertheless, distinct subunits are seen readily in the three-dimensional views, as well as in projection (Fig. 7) or sections (Fig. 8). Using longitudinal and perpendicular sections through protofilaments, two different intermolecular contact regions can be examined. Figure 8(b) shows clearly a more extensive and a less extensive contact region alternating every 42 Å. It is likely that these represent a strong internal α–β bonding domain and a weaker dimer–dimer bonding domain, respectively. In the area of the extensive bonding there appears a hole or a cleft reaching into one subunit which obstructs the α–β dimer contacts in some views. This cleft probably accounts also for the apparent bifurcation of one of the subunits visible in some sections or in projections. A perpendicular section is shown in Figure 8(c), which includes the cleft marked with a D. The accumulation of

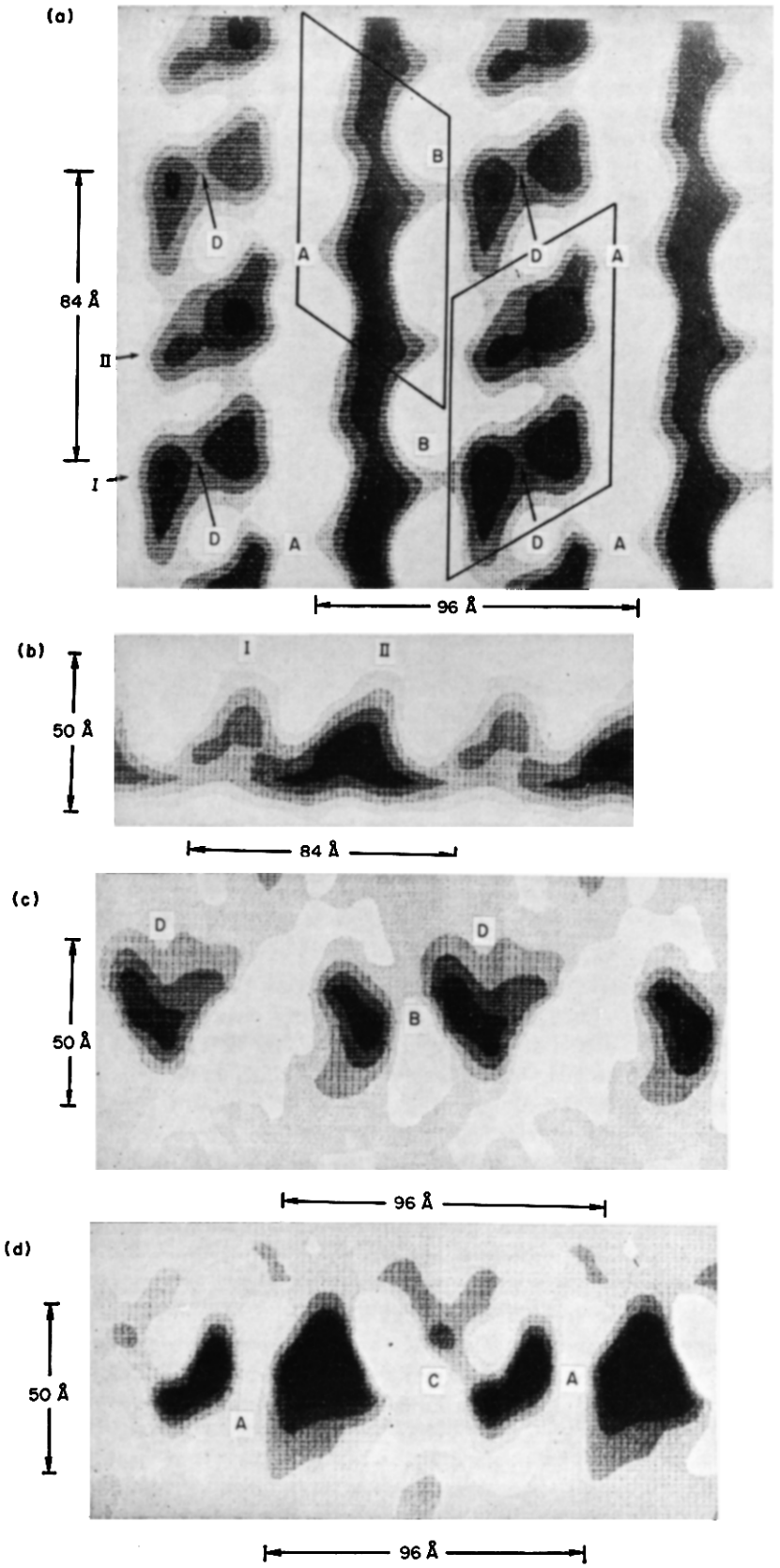
(a)
84 Å
II
I
D
A
B
96 Å
(b)
50 Å
84 Å
(c)
50 Å
96 Å
(d)
50 Å
C
96 Å

stain in this cleft causes the subunit to split in projection (Fig. 7). Figure 8(a) is a slice parallel to the sheet at 9 Å above the central section. Here the cleft is clearly visible as a hole passing nearly through the subunit and marked by a D. In the other tubulin subunit of the same protofilament approximately 40 Å away is seen a weaker cleft demonstrating that in spite of differences between monomer units homologous regions can be readily identified.

Contacts, also seen by Baker & Amos (1978), have been labeled A, B and C in Figure 7 and are shown in section in Figure 8(a), (c) and (d). The strong contact at A in projection is seen in Figure 8(d) as an approach of adjacent monomers at about the central level of the sheet. Contact B from Figure 8(a) and (c) is seen as adjacent monomers in contact at a level about 9 Å above the plane of the sheet. The weakest contact C results from an area of stain exclusively above the plane of the sheet (over the C, Fig. 8(d)) as well as a filling in of the hole at the location of C in Fig. 8(d) but not evident at this contour level. The single subunits have one rather elongated dimension which we estimate to be about 70 Å. This longest diameter of each molecule is not perpendicular to the plane of the sheet, but at an angle of approximately 30° (Fig. 6(a) and (b)). Neighboring monomers of tubulin in a protofilament seem to be arranged slightly eccentric to the main protofilament axis and slightly turned relative to each other although the difference in adjacent monomers cannot be completely accounted for by a rotation of one relative to the other. The different appearance of α and β in the normal projection is probably not only due to the cleft and bifurcation in one subunit, but also to the orientation of the monomers along a protofilament.

At this point it is important to note that all the contours for protein represent excluded stain, and some underestimates of dimensions are possible due to positive staining effects. Also the contouring level is only capable of showing rather solid protein area, while finer features are lost in the stain which cannot resolve structural detail beyond about 20 Å. Furthermore, one must be aware that information in the z direction (perpendicular to the sheet) is not fully determined, since we are missing

---

FIG. 8. Sections through the 3-dimensional reconstruction. Section (a) is a section in the plane of the sheets; other sections are perpendicular to the plane of the sheets at positions indicated in Fig. 7.

(a) Section in the plane of the sheet 9 Å above the central plane. Two protofilaments are intersected approximately through their central axis, the other 2 are only cut about 18 Å above their centers and appear therefore much narrower. The cleft (D) is very prominent in this section extending across the protofilaments. Contact region B of Fig. 7 is evident strongly at this level while region A is not contrasted as well due to the different positions of these contacts.

(b) Section along a protofilament approximately through the center (2 unit cells long). Two different types of subunit contacts are distinguishable with the more extensive contact presumably within an $\alpha\beta$ dimer. Subunit I is smaller in this Figure because referring to Fig. 7 it is more extended in a direction perpendicular to this section.

(c) Section through 4 protofilaments. The cleft is visible in this Figure as a depression in the top of one subunit. The contact B is seen as a region where the adjacent protofilaments are quite close and lies above the central plane.

(d) Section through 4 protofilaments along the middle of crossbridges A and C. Feature A is seen as an area where the subunits are close together excluding stain from this area. While actual contact is not resolved we consider it very likely that bonds are formed in this region. In the area marked C, corresponding to the C of Fig. 7, it is apparent that there is a low density feature in this region. Not apparent at this contour level is that the amount of stain present in this region is less than the corresponding large hole of Fig. 8(c). The presence of a contact region seen at C in projection is thus a combination of these 2 features.

information inside the 60° cone, namely the whole (0,0) z^* lattice line. However, this is not a major deficiency since there are data available to 20 Å resolution in the z direction for all maxima except for (0,0), (1,0), (0,1) and ($\pm$1,1). The (0,0) line only affects the average density of each slice parallel to the plane of the sheet. The (1,0) and (0,1) lines are of course equivalent and sampled to about 1/60 Å. The ($\pm$1,1) lines are weak within the measured range. Possibly small-angle X-ray diffraction could be used to investigate these regions, as done by Henderson & Unwin (1975).

Reconstructions of the three-dimensional transform, where the step of enforcing the 2-fold screw axis was omitted, showed essentially the same features as those presented here. Although the contoured stain-excluding surface was less smooth due to the less efficient use of data, the general shape of either subunit has the same appearance as in the reconstructions that made use of the screw axis symmetry.

4. Discussion

We have investigated the structure of tubulin to 20 Å when polymerized into zinc-induced sheets. We were able to show the α and β chains of tubulin as two distinctly different asymmetric units arranged alternating along the protofilaments. Alternating protofilaments are related by a 2-fold screw axis to each other, as suggested earlier on the basis of two-dimensional reconstructions (Crepeau *et al.*, 1978). This fact coupled with the observation that the protofilaments are staggered by about 15 Å with respect to the plane of the sheet accounts for the flat "pleated sheet" structure of tubulin arrays in the presence of zinc that cancels the curvature found in microtubules. In contrast, the 13 to 14 protofilaments in microtubules and their precursor sheets are aligned in parallel and therefore retain the required curvature for a cylindrical surface. Further three-dimensional analysis of those structures will be necessary to specify more precisely the relationship between protofilaments in microtubules compared to the zinc-induced sheets. Initial comparisons of two-dimensional projections indicate a similar appearance for protofilaments in the two cases (Crepeau *et al.*, 1978; Baker & Amos, 1978). Comparisons of the three-dimensional appearance of the tubulin protofilaments in zinc-induced sheets with three-dimensional microtubule models (Amos & Klug, 1974; Mandelkow *et al.*, 1977) are also consistent insofar as can be judged at the level of resolution now available. Presumably the somewhat triangular appearance seen for the protofilaments in cross section (evident most clearly in Fig. 6(a), top) would correspond to an orientation in microtubules with the wider triangular edge at the external surface. If Figure 6(a) is compared with Figure 4(b) of Mandelkow *et al.* (1977) the bilobed appearance they refer to is evident in subunits I and II of Figure 6(a) lending weight to the identification of this surface as being exterior in the microtubules. The apparent handedness of the protofilaments is also consistent in these Figures.

Our results also suggest a pairing of morphological units along a given protofilament (Fig. 8(b)). Probably, this represents the different strength of the interchain bonding within an $\alpha\beta$ dimer and the interactions between two different dimers of tubulin, since tubulin occurs in dilute solution predominantly as $\alpha\beta$ dimers. However, features in the interior of a protein are difficult to trace by negative stain, and only indirect arguments can be made. The protofilaments appear as quite compact tubes twisted on a narrow helix-like backbone. Stain penetrates into the intermolecular regions and contours single subunits sharply. What the α–β differences mean in terms

of differences in amino acid sequence or polypeptide chain folding cannot be deduced at this stage. Since we could find a more extensive pairing in the same contact area of many normal projections of single individual sheets and in planes from the three-dimensional reconstruction (e.g. Fig. 8(b)), the dimer arrangement shown in Figure 7 was indicated. In consideration of the two types of subunits the major differences relate to the presence of the clefts and the spreading of the I subunit in Figure 8(a). The contact areas may also be important structures in the maintenance of normal microtubules, and future studies will be needed to clarify this point.

Concerning the cleft, there are several possible explanations for the stain penetrating more deeply into one of the subunits. The most obvious one is that there is a pocket which accumulates stain. Alternatively, it could be an area of the polypeptide with residues that bind uranyl acetate very specifically, in what has been termed a "positive staining" artifact (Unwin, 1975). Some spurious generation of this cleft, such as by enforcing the screw axis, is very unlikely, since in reconstructions lacking an enforced screw axis its appearance was even more predominant. Most likely it is a true cleft which divides that subunit into two domains, but it might be exaggerated by positive staining effects. It is certainly a strong feature of negatively stained tubulin. A splitting of one subunit was also observed in normal microtubule precursor sheets (Crepeau *et al.*, 1978) and elements of a similar effect were very prominent even at lower resolution (Erickson, 1974).

It is clear that in this study we are at the limit of the potential of the negative staining technique for high resolution structural work. In addition to positive staining there are the limitations given by the size of the stain molecules themselves. Based on these considerations the contouring of reconstructions of any negatively stained protein must be interpreted very carefully. We therefore stress only the size of the cleft and the subunit elongation as real differences between α and β subunits. In other respects the general shape of the two types of subunits is very similar, although they are rotated relative to each other. It will be of considerable interest in this context to see how the structure of zinc-sheets prepared in glucose without stain (Unwin & Henderson, 1975) will compare to the one presented here and work is underway along these lines. Furthermore, if one can obtain large and very well-ordered sheets, it should be possible to obtain data at much higher resolution. An interesting approach will also be to prepare zinc–tubulin sheets without the microtubule-associated proteins which were found to be also involved in the polymerization of zinc-induced sheets (Gaskin & Kress, 1977). Amos (1977) observed 96 nm repeats in microtubules that were polymerized in the presence of microtubule-associated proteins. In zinc-induced sheets long distance repeats have not been consistently observed. Preliminary studies in our laboratory on tubulin, with microtubule-associated proteins removed by chromatography on a phosphocellulose column, revealed the same reciprocal lattice, but a slightly different reconstruction. Therefore, there is probably some higher order contribution of low spatial frequency information contained in our reconstruction, but it appears averaged and distributed over the different subunits. Since no effort was made to remove microtubule-associated proteins from the samples used in the work presented here, the structural details of tubulin presented in the three-dimensional reconstructions may include contributions from associated proteins.

This work was supported primarily by National Institutes of Health grant GM24800 and also by grant CA14454 and National Science Foundation grant PCM76-16760. We thank B. McEwen for discussions and help with the tubulin preparations, G. Dykes for help with the

various computer operations, E. Fram for preparing the computer program for graphic display of the three-dimensional reconstruction and C. Akey for comments on the manuscript.

REFERENCES

Amos, L. A. (1977). *J. Cell Biol.* **72**, 642–654.
Amos, L. A. & Klug, A. (1974). *J. Cell Sci.* **14**, 523–549.
Amos, L. A., Linck, R. W. & Klug, A. (1976). In *Cell Motility*, pp. 847–867, Cold Spring Harbor Laboratory, New York.
Baker, T. S. & Amos, L. A. (1978). *J. Mol. Biol.* **123**, 89–106.
Bryan, J. & Wilson, L. (1971). *Proc. Nat. Acad. Sci., U.S.A.* **68**, 1762–1766.
Chasey, D. (1972). *Exp. Cell Res.* **74**, 140.
Cleveland, D. W., Hwo, S.-Y. & Kirschner, M. W. (1977). *J. Mol. Biol.* **116**, 227–247.
Cohen, C., Harrison, S. C. & Stephens, R. E. (1971). *J. Mol. Biol.* **59**, 375–380.
Cohen, C., DeRosier, D., Harrison, S., Stephens, R. E. & Thomas, J. (1975). *Ann. N.Y. Acad. Sci.* **253**, 53–59.
Crepeau, R. H., McEwen, B., Dykes, G. & Edelstein, S. J. (1977). *J. Mol. Biol.* **116**, 301–315.
Crepeau, R. H., McEwen, B. & Edelstein, S. J. (1978). *Proc. Nat. Acad. Sci. U.S.A.* **75**, 5006–5010.
Crowther, R. A., Amos, L. A., Finch, J. T., DeRosier, D. J. & Klug, A. (1970). *Nature (London)*, **226**, 421–425.
DeRosier, D. J. & Klug, A. (1968). *Nature (London)*, **217**, 130–134.
Erickson, H. P. (1974). *J. Cell Biol.* **60**, 153–167.
Erickson, H. P. (1975). *Ann. N.Y. Acad. Sci.* **253**, 60–77.
Erickson, H. P. & Klug, A. (1971). *Phil. Trans. Roy. Soc. ser. B.*, **261**, 105–118.
Gaskin, F. & Kress, Y. (1977). *J. Biol. Chem.* **252**, 6918–6924.
Grimstone, A. V. & Klug, A. (1966). *J. Cell Sci.* **1**, 351–362.
Henderson, R. & Unwin, P. N. T. (1975). *Nature (London)*, **257**, 28–32.
Horne, R. W. & Ronchetti, P. (1974). *J. Ultrastruct. Res.* **47**, 361–383.
Larsson, H., Wallin, M. & Edström, A. (1976). *Exp. Cell Res.* **100**, 104–110.
Lowry, O. H., Rosebrough, N. J., Farr, A. L. & Randall, R. J. (1951). *J. Biol. Chem.* **193**, 265–275.
Luduena, R. F. & Woodward, D. O. (1973). *Proc. Nat. Acad. Sci., U.S.A.* **70**, 3594–3598.
Mandelkow, E., Thomas, J. & Cohen, C. (1977). *Proc. Nat. Acad. Sci., U.S.A.* **74**, 3370–3374.
Murphy, D. B., Vallee, R. B. & Borisy, G. G. (1977). *Biochemistry*, **16**, 2696–2700.
Pease, D. C. (1975). *Micron.* **6**, 85–92.
Sloboda, R. D., Dentler, W. L. & Rosenbaum, J. L. (1976). *Biochemistry*, **15**, 4497–4505.
Unwin, P. N. T. (1975). *J. Mol. Biol.* **98**, 235–242.
Unwin, P. N. T. & Henderson, R. (1975). *J. Mol. Biol.* **94**, 425–440.
Vallee, R. B. & Borisy, G. G. (1978). *J. Biol. Chem.* **253**, 2834–2845.
Weingarten, M. D., Lutes, M. M., Littman, D. R. & Kirschner, M. W. (1974). *Biochemistry*, **13**, 5529–5537.
Weisenberg, R. C. (1972). *Science*, **177**, 1104–1105.